Mon. Not. R. Astron. Soc. **386,** 324–336 (2008) doi:10.1111/j.1365-2966.2008.13042.x

Discovery of an open cluster with a possible physical association with a planetary nebula

C. Bonatto,[1⋆] E. Bica[1] and J. F. C. Santos Jr[2]

[1]*Departamento de Astronomia, Universidade Federal do Rio Grande do Sul, Av. Bento Gonçalves 9500, Porto Alegre 91501-970, RS, Brazil*
[2]*Departamento de Física, ICEx, Universidade Federal de Minas Gerais, Av. Antônio Carlos 6627, Belo Horizonte 30123-970, MG, Brazil*

Accepted 2008 January 26. Received 2008 January 18; in original form 2007 December 19

ABSTRACT

We report the discovery of a new open cluster (OC) in the Galaxy at $\ell = 167\overset{\circ}{.}0$ and $b = -1\overset{\circ}{.}0$. Its field includes the planetary nebula (PN) PK 167−0.1. We study the possible associations of the PN/OC pairs NGC 2818/2818A, NGC 2438/M 46 (NGC 2437), PK 6+2.5/NGC 6469, as well as of the PN PK 167−0.1 with New Cluster 1. The analyses are based on near-infrared colour–magnitude diagrams (CMDs) and stellar radial density profiles. NGC 6469 is located in a heavily contaminated bulge field. The CMD morphology, especially for the latter two cases, is defined with a field-star decontamination algorithm applied to the 2MASS *J*, *H* and K_s photometry. Field decontamination for the OCs NGC 2818A and M 46 produced better defined CMDs and more accurate cluster parameters than in the literature. Those pieces of evidence point to M 46 as physically associated with the PN NGC 2438. The same occurs for the OC NGC 2818A and the PN NGC 2818; however, previous radial velocity arguments indicate that they are not associated. The OC NGC 6469 does not appear to be associated with the PN PK 6+2.5, which probably belongs to the bulge. Finally, the distance of the OC New Cluster 1 is consistent with a physical association with the PN PK 167−0.1.

Key words: planetary nebulae: general – open clusters and associations: general.

1 INTRODUCTION

Planetary nebulae (PNe) are late stages in stellar evolution, occurring for stars with mass in the range 1–6.5 $M_\odot$ (Weidemann 2000), possibly with the upper limit at ∼8 $M_\odot$. Most of the difficulty in understanding such stages that lead to PNe is associated with the determination of the PN distance and its progenitor mass. Probably, the largest source of error is the distance which, in most cases, is known with a ∼50 per cent uncertainty (e.g. Zhang 1995), or more. However, both problems can be minimized if the PN is physically associated with a star cluster. Star cluster distances, in general, can be determined with a high precision and, in the case of physical association, the PN progenitor mass can be assumed to be ≈10 per cent larger than that of the turnoff (TO), stars referred to by Meynet, Mermilliod & Maeder (1993) as red-TO objects. Exceptions are the cases where mass transfer from a close binary is involved. In fact, recent radial velocity measurements, although restricted to relatively small samples, suggest that more than 90 per cent of the central stars in PNe might have companions (e.g. Moe & De Marco 2006).

Since the early observation of the PN NGC 2438, which is surrounded by stars of the open cluster (OC) M 46 (NGC 2437), photometric and spectroscopic methods have been developed to test physical associations between such objects. Žiž Novský (1975) published a list of 10 OCs with nearby projected PNe. Majaess, Turner & Lane (2007) provided a list of 13 possible physical associations and an additional list of 17 angular coincidences ($\Delta R < 15$ arcmin). They also present physical criteria for membership based on similarities in velocity, reddening and the ratio of estimated distances.

Majaess et al. (2007) reviewed theoretical and observational aspects of stellar evolution to impose limiting parameters for PNe to be OC members. Many coincidences can be discarded if the PN is a bulge member (Žiž Novský 1975), as indicated by position along the disc and radial velocities. OCs younger than 28 Myr produce type II supernova. The short-lived PN phase varies from 10^3 to 10^5 yr, according to the progenitor mass (Köppen & Acker 2000; Schönberner & Blöcker 1996), and does not favour associations. PNe observed in globular clusters (e.g. Köppen & Acker 2000) imply that their TOs at $\lesssim$1 $M_\odot$ are below the lower mass limit for PN progenitors. This invokes mass transfer in binary systems to produce PN in globular clusters. Moe & De Marco (2006), Soker (2006) and Zijlstra (2007) presented a scenario where most PNe arise from binaries. Consequently, care is necessary because the cluster age may not correspond to the PN mass progenitor.

Among the list of 30 PN/OC coincidences provided by Majaess et al. (2007), we selected the PN/OC pairs NGC 2818/2818A and NGC 2438/M 46 (NGC 2437). We also

⋆E-mail: charles@if.ufrgs.br

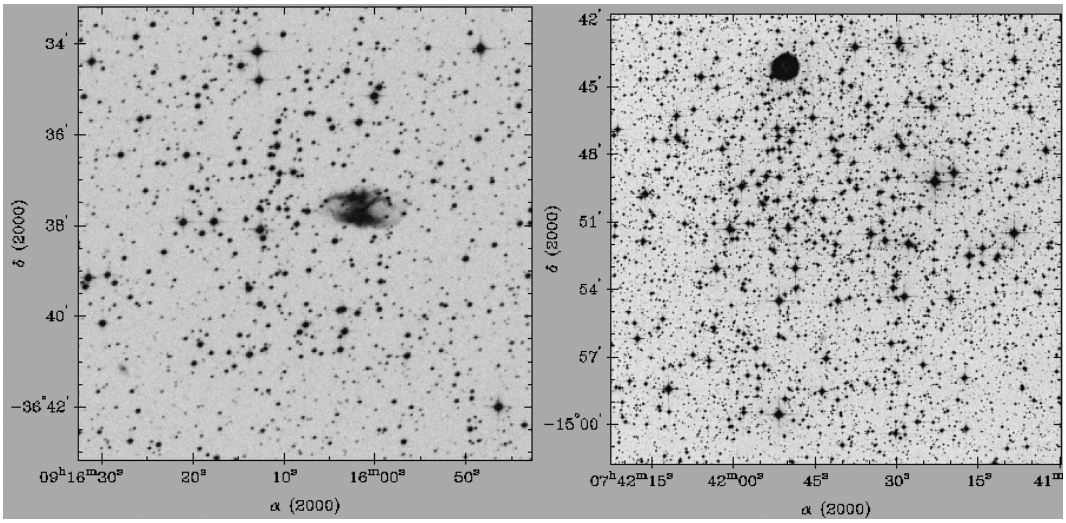

Figure 1. Left-hand panel: 10 × 10-arcmin^2 XDSS *R* image of the OC NGC 2818A and the PN NGC 2818. Right-hand panel: 20 × 20-arcmin^2 XDSS *R* image of the OC M 46 and the PN NGC 2438. Images centred on the 2MASS coordinates (columns 5 and 6 of Table 1). North to the top and east is towards the left-hand side.

include PK 6+2.5/NGC 6469 and PK 167−0.1, which is projected in the field of an as-yet unknown star cluster. We name this low-contrast cluster New Cluster 1. In the present paper we derive accurate distances to these OCs, which in turn, can be used to investigate the possible associations.

Besides the investigation on possible PN/OC associations, the present work also serves to provide reliable astrophysical parameters of scarcely studied OCs, as well as to characterize a new one. Such data are important both to studies of the disc structure and to constrain theories of molecular cloud fragmentation, star formation, as well as stellar and dynamical evolutions. The present work employs near-infrared *J*, *H* and K_s photometry obtained from the Two Micron All Sky Survey (2MASS)[1] Point Source Catalogue (PSC). The spatial and photometric uniformity of 2MASS, which allow extraction of large surrounding fields that provide high star count statistics, have been important to derive cluster parameters and probe the nature of stellar overdensities (e.g. Bica, Bonatto & Camargo 2007).

To this purpose we have developed quantitative tools to disentangle cluster and field stars in colour–magnitude diagram (CMDs), in particular two different kinds of filters. Basically we apply (i) field-star decontamination to uncover cluster evolutionary sequences from the field, which is important to derive reddening, age and distance from the Sun and (ii) colour–magnitude filters, which proved to be essential for building intrinsic stellar radial density profiles (RDPs), as well as luminosity and mass functions (MFs). In particular, field-star decontamination constrains more the age and distance, especially for low-latitude OCs (Bonatto et al. 2006b). These tools were applied to OCs and embedded clusters to enhance main sequence (MS) and/or pre-MS with respect to the field (Bonatto & Bica 2006; Bica & Bonatto 2005; Bonatto & Bica 2005; Santos, Bonatto & Bica 2005; Bonatto, Santos & Bica 2006a; Bonatto et al. 2006c). They were useful in the analysis of faint and/or distant OCs (Bica, Bonatto & Dutra 2003, 2004; Bica & Bonatto 2005; Bica, Bonatto & Blumberg 2006a). In addition, more constrained structural parameters, such as core and limiting radii (R_c and R_l, respectively), and MF slopes, have been derived from colour–magnitude-filtered photometry (e.g. Bonatto & Bica 2005).

This paper is organized as follows. Section 2 contains basic properties and reviews literature data (when available) on the possible PN/OC associations. In Section 3 we present the 2MASS photometry, build CMDs, discuss the field-star decontamination and derive cluster fundamental parameters. Section 4 describes cluster structure by means of stellar RDPs and mass density profiles (MDPs). In Section 5 MFs are built and cluster masses are estimated. In Section 6 aspects related to the structure of the present objects are discussed. In Section 7 we discuss membership considerations. Concluding remarks are given in Section 8.

2 THE PRESENT POSSIBLE PN/OC ASSOCIATIONS

In Fig. 1 we show optical XDSS[2] images of NGC 2818/2818A (left-hand panel, *R* band) and NGC 2438/M 46 [right-hand panel, Digitized Sky Survey (DSS) *B* band]. Fig. 2 contains a DSS *B* image of PK 6+2.5/NGC 6469 (left-hand panel) and an XDSS *R* image of PK 167−0.1/New Cluster 1 (right-hand panel).

Table 1 provides fundamental data on the OCs. WEBDA[3] coordinates are in columns 2 and 3; column 4 gives the 2MASS extraction radii (Section 3). However, since the RDPs (Section 4) built with the 2MASS coordinates presented a dip at the centre; new coordinates were searched to maximize the central density of stars. The optimized central coordinates and the corresponding Galactic longitude and latitude are given in columns 5–8 of Table 1. Age, central reddening, distance from the Sun and Galactocentric distance based on 2MASS data (Section 3.2) are given in columns 9–12. Additional designations are in column 13.

Positional data of the PNe are given in Table 2, where we also include the angular separation with respect to the OC centre and its

[1] The 2MASS All Sky data release (Skrutskie et al. 1997), available at http://www.ipac.caltech.edu/2mass/releases/allsky/.

[2] Extracted from the Canadian Astronomy Data Centre (CADC), at http://cadcwww.dao.nrc.ca/.

[3] obswww.univie.ac.at/webda – Mermilliod & Paunzen (2003).

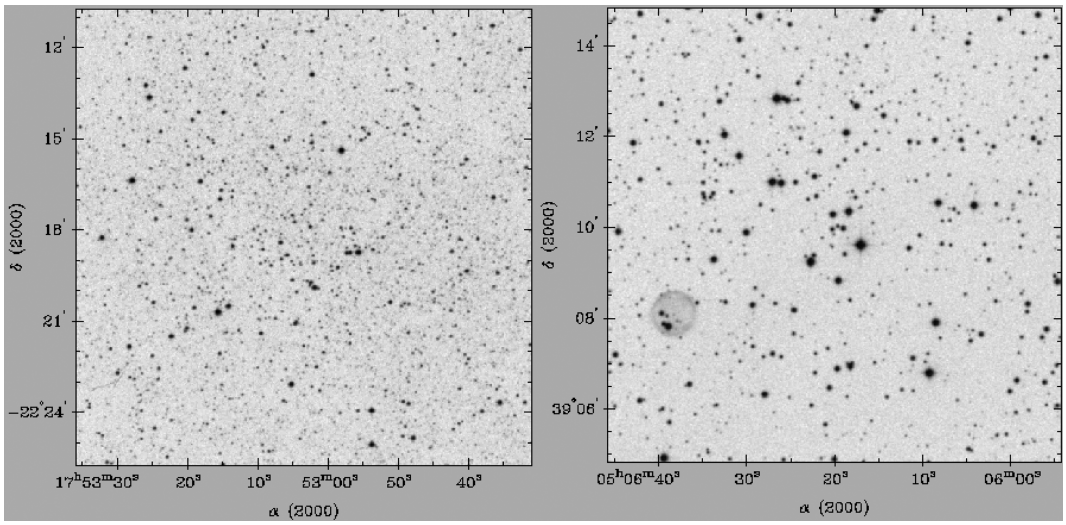

Figure 2. Left-hand panel: 15 × 15-arcmin^2 DSS *B* image of the OC NGC 6469 and the PN PK 6+2.5. The nearly stellar PN is located close to the lower right-hand corner (see equatorial coordinates in Table 2). Right-hand panel: 10 × 10-arcmin^2 XDSS *R* image of the OC New Cluster 1 and the PN PK 167−0.1.

relation with the OC's core and limiting radii (Section 7). Coordinates are taken from SIMBAD.[4]

Additional information on the possible pairs, related to the present work, are summarized below.

2.1 The pair NGC 2818/2818A

Since NGC 2818 refers to the original description of the PN, we adopt NGC 2818A as the OC designation. Majaess et al. (2007) classify this pair as a suspected physical association. Pedreros (1989) derived a distance from the Sun $d_\odot = 2300$ pc and a reddening $E(B-V) = 0.18$, which are consistent with $d_\odot = 2660 \pm 830$ pc (Zhang 1995) and $E(B-V) = 0.28 \pm 0.15$ (Tylenda et al. 1992) for the PN. Although earlier studies pointed to a similar radial velocity between cluster stars and the PN, Mermilliod et al. (2001) give $V_r = 20.7 \pm 0.3\,\mathrm{km\,s^{-1}}$ for 15 red giants of NGC 2818A, while for the PN $V_r = -0.9 \pm 2.9\,\mathrm{km\,s^{-1}}$ (Durand, Acker & Zijlstra 1998) and $V_r = -1 \pm 3\,\mathrm{km\,s^{-1}}$ (Meatheringham, Wood & Faulkner 1988). Mermilliod et al. (2001) favour a projection effect. As for NGC 2818A, available age estimates are 1 Gyr (Mermilliod et al. 2001), 930 Myr (Lata et al. 2002) and 794 Myr (Tadross et al. 2002). Additionally, Tadross et al. (2002) provide for NGC 2818A $d_\odot = 2.9$ kpc, cluster mass $m \approx 288\,M_\odot$ and the limiting radius $R_l = 3.9$ pc. Mermilliod et al. (2001) and Lata et al. (2002) derived $E(B-V) = 0.18$, in agreement with the $E(B-V) = 0.20$ of Tadross et al. (2002).

2.2 The pair NGC 2438/M 46 (NGC 2437)

Based on the available evidence, Majaess et al. (2007) do not exclude the physical association. The distance from the Sun and reddening of the PN are $d_\odot = 1775 \pm 630$ pc (Zhang 1995) and $E(B-V) = 0.17 \pm 0.08$ (Tylenda et al. 1992), respectively. The isochrone fit with 2MASS photometry by Majaess et al. (2007) provided for the OC M 46 $d_\odot = 1700 \pm 250$ pc, $E(B-V) = 0.13 \pm 0.05$ and age = 22×10^7 Myr. Early determinations of radial velocity indicated differences of $\approx$30 km s^{-1} (Majaess et al. 2007, and references therein), which suggest spatial coincidence. However, the most recent study on radial velocity of cluster stars and PN (Pauls & Kohoutek 1996) shows comparable values, reinforcing the possible physical association. Additional available data on the OC M 46 are age = 250 Myr, $d_\odot = 1.5$ kpc, core $R_c = 2.27 \pm 0.13$ pc and limiting radii $R_l = 11.6$ pc (Nilakshi, Pandey & Mohan 2002); $E(B-V) = 0.15$, age = 144 Myr, $d_\odot = 1.4$ kpc, $R_c = 7.2$ arcmin and $R_l = 23$ arcmin (Kharchenko et al. 2005); $R_c = 4.2 \pm 0.3$ pc and $R_l = 11$ pc (Sharma et al. 2006).

2.3 The pair PK 6+2.5/NGC 6469

The PN is also known as M 1−31, Ve 3−59, ESO 589−PN 16 and PNG 006.4+02.0. No distance to the PN is available, but Durand et al. (1998) provide $V_r = 68.8 \pm 1.8\,\mathrm{km\,s^{-1}}$. The PN is projected on the bulge, which decreases the possibility of a physical association. Kharchenko et al. (2005) obtained for the OC NGC 6469 age = 230 Myr, $E(B-V) = 0.30$, $d_\odot = 0.55$ kpc, $R_c = 5.4$ arcmin and $R_l = 9$ arcmin.

2.4 The pair PK 167−0.1/New Cluster 1

The PN is also known as A 55 7 and PNG 167.0−00.9. The available distance and radial velocity estimates are $d_\odot = 1780$ pc (Phillips 2004) and $V_r = 58.2 \pm 6.5\,\mathrm{km\,s^{-1}}$ (Durand et al. 1998), respectively. The OC New Cluster 1 was found by one of us (E. Bica) on DSS images, and is analysed for the first time.

3 2MASS PHOTOMETRY

J, *H* and K_s 2MASS photometry was extracted in circular fields centred on the optimized coordinates of the objects (columns 5 and 6 of Table 1) using VizieR.[5] Previous analyses of OCs in different environments (Section 1) have shown that as long as no other populous cluster is present in the field, and differential absorption is not prohibitive, wide extraction areas provide the required statistics for

[4] http://simbad.u-starsbg.fr/simbad/.

[5] http://vizier.u-strasbg.fr/viz-bin/VizieR?-source=II/246.

Table 1. General data on the clusters.

	WEBDA							Derived from 2MASS				
Cluster	α(2000)	δ(2000)	$R_{\rm ext}$	α(2000)	δ(2000)	ℓ	b	Age	$E(B-V)$	$d_\odot$	$R_{\rm GC}$	Alternative names
	($^{\rm h\,m\,s}$)	($^\circ$ $'$ $''$)	(arcmin)	($^{\rm h\,m\,s}$)	($^\circ$ $'$ $''$)	($^\circ$)	($^\circ$)	(Myr)		(kpc)	(kpc)	
(1)	(2)	(3)	(4)	(5)	(6)	(7)	(8)	(9)	(10)	(11)	(12)	(13)
NGC 2818A	09:16:01	−36:37:30	80	09:16:07.7	−36:38:09.6	262.0	+8.6	1000 ± 100	0.10 ± 0.03	2.8 ± 0.1	8.1 ± 0.2	ESO 372−13,Hen 2−23,PK 261+08
M 46	07:41:46	−14:48:36	80	07:41:41.1	−14:51:45.0	231.9	+4.0	250 ± 50	0.10 ± 0.03	1.5 ± 0.1	8.3 ± 0.2	NGC 2437,Mel−75,Cr 159,OCl−601
NGC 6469	17:53:13	−22:19:11	45	17:53:03.4	−22:18:14.4	6.55	+1.97	250 ± 50	0.58 ± 0.06	1.1 ± 0.1	6.1 ± 0.2	Mel−182,Cr 353,OCl−21,ESO 589 SC 18
New Cluster 1	–	–	60	05:06:20	+39:09:50.0	167.0	−1.0	1000 ± 100	0.29 ± 0.03	1.7 ± 0.1	8.9 ± 0.2	

Notes: Columns 2 and 3: coordinates from WEBDA; column 4: extraction radius; column 10: reddening in the cluster's central region (Section 3.2); column 12: $R_{\rm GC}$ for $R_\odot = 7.2$ kpc (Bica et al. 2006b).

a consistent field-star characterization in terms of colour and luminosity distribution. Thus, the 2MASS extraction radii (column 4 of Table 1) are significantly larger than the limiting radii (Section 4 and column 7 of Table 4) of the present objects. For decontamination purposes, comparison fields were selected within wide rings centred on the cluster coordinates and beyond their limiting radii. As a photometric quality constraint, 2MASS extractions were restricted to stars with magnitudes (i) brighter than those of the 99.9 per cent PSC completeness limit[6] in the cluster direction and (ii) with errors in J, H and $K_{\rm s}$ smaller than 0.2 mag. The 99.9 per cent completeness limits are different for each cluster, varying with Galactic coordinates. The fraction of stars with J, H and $K_{\rm s}$ uncertainties smaller than 0.06 mag is ≈75 per cent (NGC 6469), ≈94 per cent (New Cluster 1), ≈73 per cent (NGC 2818A) and ≈93 per cent (M 46). A typical distribution of uncertainties as a function of magnitude, for objects projected towards the central parts of the Galaxy, can be found in Bonatto & Bica (2007). Reddening transformations use the relations $A_J/A_V = 0.276$, $A_H/A_V = 0.176$, $A_{K_{\rm s}}/A_V = 0.118$ and $A_J = 2.76 \times E(J-H)$ (Dutra, Santiago & Bica 2002), for a constant total-to-selective absorption ratio $R_V = 3.1$.

3.1 Field-star-decontaminated CMDs

$J \times (J-H)$ and $J \times (J-K_{\rm s})$ CMDs of central extractions of the clusters are shown in Figs 3 and 4. Features present in the central CMDs and those in the respective comparison field (top and middle panels), show that field stars contribute in varying proportions to the CMDs, especially for the bulge-projected OC NGC 6469 (Fig. 4). Nevertheless, when compared to the equal-area comparison field extractions, cluster-like sequences are suggested, especially for M 46, NGC 2818A and 6469 (the blue sequence).

To objectively quantify the field-star contamination in the CMDs we apply the statistical algorithm described in Bonatto & Bica (2007). It measures the relative number densities of probable field and cluster stars in cubic CMD cells whose axes correspond to the magnitude J and the colours $(J-H)$ and $(J-K_{\rm s})$. These are the 2MASS colours that provide the maximum variance among CMD sequences for OCs of different ages (e.g. Bonatto, Bica & Girardi 2004). The algorithm (i) divides the full range of CMD magnitude and colours into a 3D grid, (ii) computes the expected number density of field stars in each cell based on the number of comparison field stars with similar magnitude and colours as those in the cell and (iii) subtracts the expected number of field stars from each cell. By construction, the algorithm is sensitive to local variations of field-star contamination with colour and magnitude (Bonatto & Bica 2007). Typical cell dimensions are $\Delta J = 0.5$, and $\Delta(J-H) = \Delta(J-K_{\rm s}) = 0.25$, which are large enough to allow sufficient star count statistics in individual cells and small enough to preserve the morphology of different CMD evolutionary sequences. As comparison field we use wide rings extracted from the region $R_{\rm l} < R \lesssim R_{\rm ext}$ around the cluster centre to obtain representative background star count statistics, where $R_{\rm l}$ is the limiting radius (Section 4). The comparison fields effectively used are located within $R = 30$–80 arcmin (NGC 2818A), $R = 40$–80 arcmin (M 46), $R = 20$–45 arcmin (NGC 6469) and $R = 10$–60 arcmin (New Cluster 1). In all cases, the inner boundary of the comparison field lies beyond the probable tidal radius (Section 4). We emphasize that the equal-area extractions shown in the middle panels of Figs 3 and 4 serve only for visual comparison

[6] Following the level 1 requirement, according to http://www.ipac.caltech.edu/2mass/releases/allsky/doc/sec6_5a1.html.

Table 2. PN coordinates and angular separation with the OCs.

PN	α(2000) ($^{\rm h}\,^{\rm m}\,^{\rm s}$)	δ(2000) ($^\circ\,'\,''$)	ℓ ($^\circ$)	b ($^\circ$)	ΔR (arcmin)	$f_{\rm c}$	$f_{\rm l}$
(1)	(2)	(3)	(4)	(5)	(6)	(7)	(8)
NGC 2818	09:16:01.7	−36:37:38.8	261.98	+8.58	1.6	0.8	0.1
NGC 2438	07:41:51.4	−14:43:54.9	231.80	+4.12	8.2	1.8	0.3
PK 6+2.5	17:52:41.4	−22:21:56.8	6.45	+2.01	6.6	6.0	0.5
PK 167−0.1	05:06:38.4	+39:08:8.6	167.04	−0.97	4.9	10.5	1.4

Notes: Columns 2–5: coordinates from SIMBAD; column 6: angular separation of the PN to the optimized cluster centre; columns 7 and 8: ratio of the PN's angular separation with the core ($f_{\rm c} = \Delta R/R_{\rm c}$) and limiting ($f_{\rm l} = \Delta R/R_{\rm l}$) radii (Section 4), respectively.

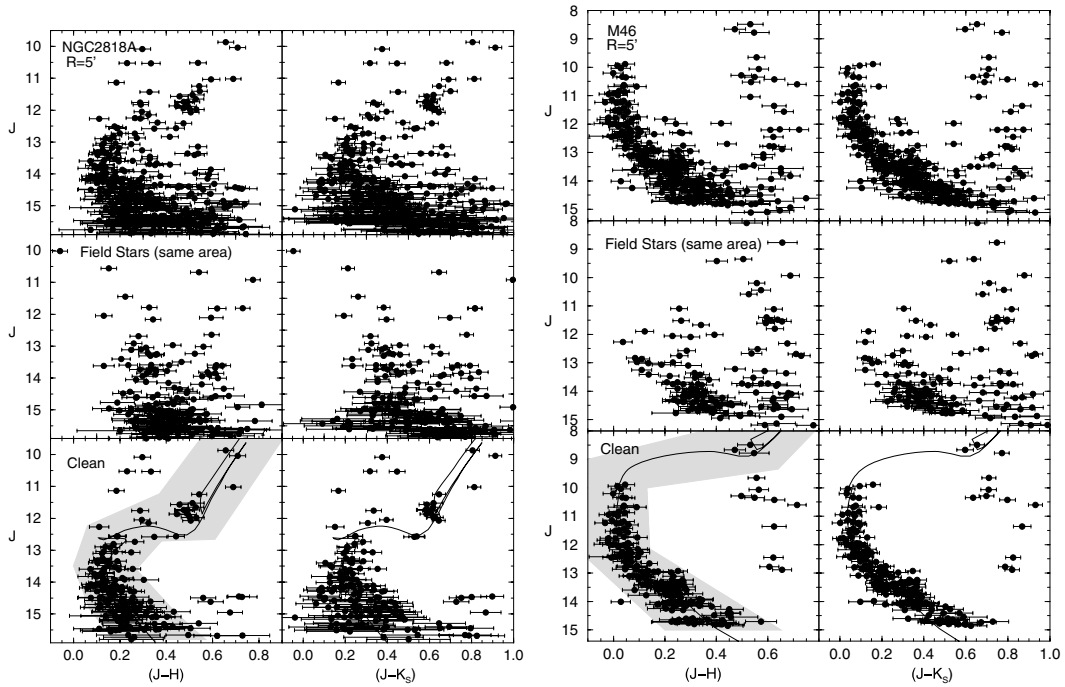

Figure 3. Left-hand side: 2MASS CMDs extracted from the $R < 5$ arcmin region of NGC 2818A. Top panels: observed photometry with the colours $J \times (J - H)$ (left-hand side) and $J \times (J - K_{\rm s})$ (right-hand side). Middle panels: equal-area extraction of the comparison field. Besides some contamination of disc stars, a populous MS and a giant clump show up. Bottom panels: decontaminated CMDs set with the 1-Gyr Padova isochrone (solid line). The colour–magnitude filter used to isolate cluster MS/evolved stars is shown as a shaded region. Right-hand side: Same, but for M 46, except for the 250-Myr Padova isochrone.

purposes. Actually, the decontamination process is carried out with the large surrounding area as described above. Further details on the algorithm, including discussions on subtraction efficiency and limitations, are given in Bonatto & Bica (2007).

The decontaminated CMDs are shown in the bottom panels of Figs 3 and 4. As expected, most of the disc contamination in NGC 2818A, M 46 and New Cluster 1 is removed, leaving stellar sequences typical of evolved/intermediate-age OCs. The centrally projected NGC 6469, on the other hand, is so heavily contaminated by bulge stars that the algorithm does not subtract all of the field stars. The residual bulge component is probably due to differential reddening in the field, since the expected Poisson residuals should be smaller. In fact, the residual bulge component (bottom panel) contains 398 stars, and the observed (top panel) contains 1893. Since the cluster sequence is significantly bluer than the bulge stars, both sequences can be unambiguously separated. We note that in all cases, essentially the same CMD features show up in both colours. New Cluster 1 has evidence of MS depletion (Fig. 4), suggesting advanced dynamical evolution.

NGC 2818A and M 46 have easy-to-detect cluster CMD sequences and, to some extent, the same applies to NGC 6469. However, the non-populous nature of New Cluster 1 requires additional statistical evidence. To this end we present in Table 3 the full statistics of the decontaminated sequences and field stars, by magnitude bins. As a caveat we note that it is more meaningful to work with isolated cluster sequences instead of the full photometric sample. The bulge residual in the CMD of NGC 6469, for instance, contains more stars per magnitude bin than the assumed cluster sequence, which would mask the decontamination statistics. In this sense, we first isolate the cluster sequences by means of appropriate colour–magnitude filters, which are used to exclude stars with colours different from those of the assumed cluster sequence. They are wide enough to accommodate cluster MS and evolved star colour distributions, allowing for the 1σ photometric uncertainties. Colour–magnitude filter widths should also account for formation or dynamical evolution-related effects, such as enhanced fractions of binaries (and other multiple systems) towards the central parts of clusters, since such systems tend to widen the MS (e.g. Hurley &

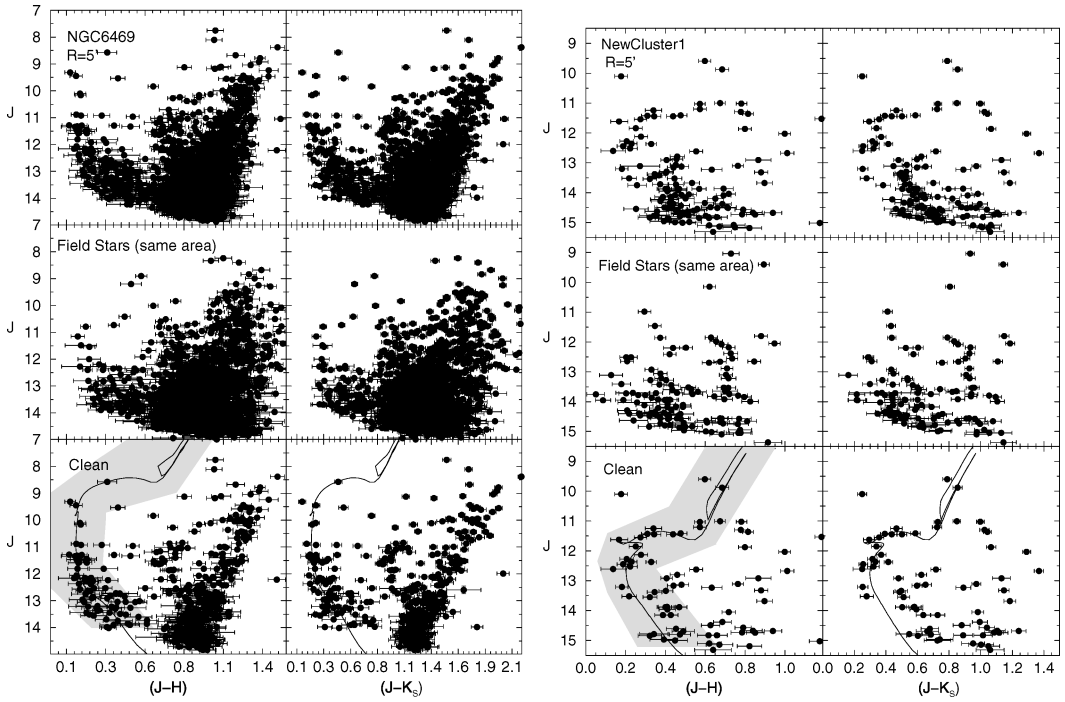

Figure 4. Same as Fig. 3 for NGC 6469 (left-hand side) and New Cluster 1 (right-hand side). Isochrones used are the 250 Myr (NGC 6469) and 1 Gyr (New Cluster 1) ones. Despite the heavy contamination by bulge stars, a blue sequence shows up in the CMD of NGC 6469. New Cluster 1 is a poorly populated IAC.

Table 3. Statistics of the field-star decontamination in magnitude bins.

	Colour–magnitude-filtered photometry																			
	NGC 2818A					M 46					NGC 6469					New Cluster 1				
ΔJ	σ_{FS}	N_{obs}	N_{cl}	$N_{1\sigma}$	FS_{unif}	σ_{FS}	N_{obs}	N_{cl}	$N_{1\sigma}$	FS_{unif}	σ_{FS}	N_{obs}	N_{cl}	$N_{1\sigma}$	FS_{unif}	σ_{FS}	N_{obs}	N_{cl}	$N_{1\sigma}$	FS_{unif}
8–9	–	–	–	–	–	0.11	3	3	1.7	0.28	0.14	1	1	1.0	0.37	–	–	–	–	–
9–10	0.14	1	1	1.0	0.22	0.25	2	2	1.4	0.39	0.31	3	3	1.7	0.45	0.29	2	2	1.4	0.45
10–11	0.34	2	2	1.4	0.10	0.30	12	12	3.5	0.53	0.74	5	5	2,2	0.46	–	–	–	–	–
11–12	0.34	18	17	4.0	0.07	0.31	22	22	4.5	0.26	1.92	14	12	3.2	0.40	0.77	11	11	3.3	0.17
12–13	1.36	20	12	2.7	0.14	0.28	43	43	6.3	0.06	2.83	36	25	4.2	0.16	1.07	7	5	1.9	0.15
13–14	1.43	31	27	4.8	0.25	1.16	72	72	6.4	0.05	7.01	67	27	3.3	0.14	2.09	19	3	0.7	0.11
14–15	3.47	78	63	7.1	0.18	3.18	85	85	5.4	0.08	–	–	–	–	–	3.35	40	12	1.9	0.08
15–16	4.51	81	36	4.0	0.09	–	–	–	–	–	–	–	–	–	–	–	–	–	–	–
All	10.95	231	158	9.9	0.12	4.97	238	182	11.6	0.07	9.20	126	73	5.9	0.12	6.42	79	33	2.7	0.09

Notes: This table provides, for each magnitude bin (ΔJ), the 1σ Poisson fluctuation (σ_{FS}) around the mean, with respect to the star counts measured in the eight sectors of the comparison field, the number of observed stars (N_{obs}) within the spatial region sampled in the CMDs shown in the top panels of Figs 3 and 4, the respective number of probable member stars (N_{cl}) according to the decontamination algorithm, the $N_{1\sigma}$ parameter and the field-star uniformity parameter. The statistical significance of N_{cl} is reflected in its ratio with the 1σ Poisson fluctuation of N_{obs} ($N_{1\sigma}$) and with σ_{FS}. The bottom line corresponds to the full magnitude range.

Tout 1998; Kerber et al. 2002; Bonatto, Bica & Santos 2005; Bonatto & Bica 2007). The colour–magnitude filters for the present objects are shown in the bottom panels of Figs 3 and 4.

Statistically relevant parameters to characterize the nature of a star cluster are: (i) $N_{1\sigma}$ which, for a given magnitude bin, corresponds to the ratio of the decontaminated number of stars to the 1σ Poisson fluctuation of the number of observed stars; (ii) σ_{FS}, which is related to the probability that the decontaminated stars result from the normal star count fluctuation in the comparison field and (iii) FS_{unif}, which measures the star count uniformity of the comparison field. See below for the precise definition of these parameters. Properties of $N_{1\sigma}$, σ_{FS} and FS_{unif}, measured in OCs and field fluctuations are discussed in Bica et al. (2007). Table 3 also provides integrated values of the above parameters, which correspond to the full magnitude range spanned by each OC. The spatial regions considered here are those sampled by the CMDs shown in the top panels of Figs 3 and 4.

CMDs of star clusters should have integrated $N_{1\sigma}$ values significantly larger than 1 (Bica et al. 2007). Indeed, this condition is met by NGC 2818A, M 46 and NGC 6469. New Cluster 1, on the other hand, occurs at the $\approx 2.7\sigma$ level, close to the lower limit observed in central directions (Bica et al. 2007). Values higher than 3σ occur as well for the $N_{1\sigma}$ measured in magnitude bins. Because of the small number of bright stars, we point out that this analysis

should be basically considered for $J \gtrsim 10$. As a further test of the statistical significance of the above results we investigate star count properties of the field stars. First, the comparison field is divided in eight sectors, each with 45° of opening angle around the cluster centre. Next, we compute the parameter $\sigma_{\rm FS}$, which is the 1σ Poisson fluctuation around the mean of the star counts measured in the eight sectors of the comparison field (corrected for the different areas of the sectors and cluster extraction). For a spatially uniform comparison field, $\sigma_{\rm FS}$ should be very small. In this context, star clusters should have the probable number of member stars ($N_{\rm cl}$) higher than $\sim 3\sigma_{\rm FS}$ to minimize the probability that $N_{\rm cl}$ results from the normal fluctuation of a non-uniform comparison field. Again, this condition is fully satisfied, in some cases reaching the level $N_{\rm cl} \sim 10\,\sigma_{\rm FS}$. The ratio decreases somewhat for New Cluster 1, but still is higher than ∼3, probably because it is almost projected against the anticentre. Finally, we also provide in Table 3 the parameter $FS_{\rm unif}$. For a given magnitude bin we first compute the average number of stars over all sectors $\langle N\rangle$ and the corresponding 1σ fluctuation $\sigma_{\langle N\rangle}$; thus, $FS_{\rm unif}$ is defined as $FS_{\rm unif} = \sigma_{\langle N\rangle}/\langle N\rangle$. Non-uniformities such as heavy differential reddening should result in high values of $FS_{\rm unif}$.

The three statistical tests applied to the present sample, i.e. (i) the decontamination algorithm, (ii) the integrated and per magnitude $N_{1\sigma}$ parameter and (iii) the ratio of $N_{\rm cl}$ to $\sigma_{\rm FS}$, produce consistent results. As for New Cluster 1, the number of decontaminated stars in each magnitude bin is significantly larger than what could be expected from field-star fluctuations. Besides, its field is rather uniform (Table 3). We conclude that New Cluster 1 is a poorly populated Gyr-class OC.

3.2 Cluster age, reddening and distance

Fundamental parameters for the present clusters are derived from CMD fits with solar-metallicity Padova isochrones (Girardi et al. 2002) computed with the 2MASS J, H and $K_{\rm s}$ filters.[7] These isochrones are very similar to the Johnson–Kron–Cousins (e.g. Bessel & Brett 1988) ones, with differences of at most 0.01 in $(J-H)$ (Bonatto et al. 2004). The decontaminated CMD morphologies (bottom panels of Figs 3 and 4) provide enough constraints to derive reliable cluster fundamental parameters, which are given in Table 1. The isochrone fits to the decontaminated cluster CMDs are shown in the bottom panels of Figs 3 and 4.

From the isochrone fit to the CMD of NGC 2818A (Fig. 3) we derive the age 1.0 ± 0.1 Gyr, reddening $E(J-H) = 0.03 \pm 0.01$ that converts to $E(B-V) = 0.10 \pm 0.02$ and $A_V = 0.31 \pm 0.07$, and $\rm d_\odot = 2.8 \pm 0.1$ kpc. We adopt $\rm R_\odot = 7.2 \pm 0.3$ kpc (Bica et al. 2006b) as the Sun's distance to the Galactic Centre to compute the OC's Galactocentric distances. The latter value was derived by means of the globular cluster spatial distribution. Besides, other recent studies gave similar results, e.g. $\rm R_\odot = 7.2 \pm 0.9$ kpc (Eisenhauer et al. 2003), $\rm R_\odot = 7.62 \pm 0.32$ kpc (Eisenhauer et al. 2005 and $\rm R_\odot = 7.52 \pm 0.10$ kpc (Nishiyama et al. 2006), with different approaches. Thus, for $\rm R_\odot = 7.2$ kpc, the Galactocentric distance of NGC 2818A is $R_{\rm GC} = 8.1 \pm 0.2$ kpc. NGC 2818A lies ≈0.9 kpc outside the solar circle. Within the uncertainties, the present age and reddening values agree with those of Lata et al. (2002) and Mermilliod et al. (2001). The distance from the Sun is the same as that in Tadross et al. (2002). The mass at the TO of NGC 2818A is $m_{\rm TO} = 2.1\,\rm M_\odot$.

[7] http://stev.oapd.inaf.it/∼lgirardi/cgi-bin/cmd.

Parameters of M 46 are the age 250 ± 50 Myr, $E(J-H) = 0.03 \pm 0.01, E(B-V) = 0.10 \pm 0.02$, and $A_V = 0.31 \pm 0.07, \rm d_\odot = 1.5 \pm 0.1$ kpc and $R_{\rm GC} = 8.3 \pm 0.2$ kpc, ≈1.1 kpc outside the solar circle. Within the uncertainties, these parameters agree with those of Majaess et al. (2007) and Nilakshi et al. (2002); the present age is about twice that of Kharchenko et al. (2005). TO mass is $m_{\rm TO} = 3.5\,\rm M_\odot$.

For the bulge-projected NGC 6469 we derive the age 250 ± 50 Myr, $E(J-H) = 0.18 \pm 0.02, E(B-V) = 0.58 \pm 0.05$ and $A_V = 1.8 \pm 0.2, \rm d_\odot = 1.1 \pm 0.1$ kpc and $R_{\rm GC} = 6.1 \pm 0.2$ kpc, ≈1.1 kpc inside the solar circle. The present age agrees with that of Kharchenko et al. (2005), but they found about twice the reddening and half the distance from the Sun. TO mass is $m_{\rm TO} = 3.5\,\rm M_\odot$.

Finally, parameters of New Cluster 1, derived for the first time, are the age 1.0 ± 0.1 Gyr, $E(J-H) = 0.09 \pm 0.01, E(B-V) = 0.29 \pm 0.03$, and $A_V = 0.9 \pm 0.1, \rm d_\odot = 1.7 \pm 0.1$ kpc and $R_{\rm GC} = 8.9 \pm 0.2$ kpc, ≈1.7 kpc outside the solar circle. TO mass is $m_{\rm TO} = 2.1\,\rm M_\odot$.

Except for the bulge-projected NGC 6469, which is located ≈1 kpc inside the solar circle, the remaining OCs are more than 1 kpc outside it.

4 CLUSTER STRUCTURE

Structural parameters are derived by means of RDPs, defined as the projected radial distribution of the number density of stars around the cluster centre.

Star clusters usually have RDPs that follow some well-defined analytical profile. The most often used are the single mass, modified isothermal sphere of King (1966), the modified isothermal sphere of Wilson (1975) and the power law with a core of Elson, Fall & Freeman (1987). Each function is characterized by different parameters that are somehow related to cluster structure. However, because the error bars in the present RDPs are significant (see below), we decided to use the analytical profile $\sigma(R) = \sigma_{\rm bg} + \sigma_0/[1 + (R/R_{\rm C})^2]$, where $\sigma_{\rm bg}$ is the residual background density, σ_0 is the central density of stars and $R_{\rm c}$ is the core radius. This function is similar to that introduced by King (1962) to describe the surface brightness profiles in the central parts of globular clusters.

In all cases we build the stellar RDPs with colour–magnitude-filtered photometry (Section 3.1). However, residual field stars with colours similar to those of the cluster are expected to remain inside the colour–magnitude filter region. They affect the intrinsic stellar RDP in a degree that depends on the relative densities of field and cluster stars. The contribution of the residual contamination to the observed RDP is statistically taken into account by means of the comparison field. In practical terms, the use of colour–magnitude filters in cluster sequences enhances the contrast of the RDP with respect to the background level, especially for objects in dense fields (e.g. Bonatto & Bica 2007).

To avoid oversampling near the centre and undersampling at large radii, RDPs are built by counting stars in rings of increasing width with distance from the centre. A typical distribution of ring widths would be $\Delta R = 0.5$, 1, 2, 5 and 10 arcmin, respectively, for $0 \leqslant R < 1$ arcmin, $1 \leqslant R < 4$ arcmin, $4 \leqslant R < 10$ arcmin, $10 \leqslant R < 30$ arcmin and $R \gtrsim 30$ arcmin. However, the number and width of the rings are adjusted to produce RDPs with adequate spatial resolution and as small as possible 1σ Poisson errors. The residual background level of each RDP corresponds to the average number of colour–magnitude-filtered stars measured in the comparison field. The R coordinate (and respective uncertainty) of each ring corresponds to

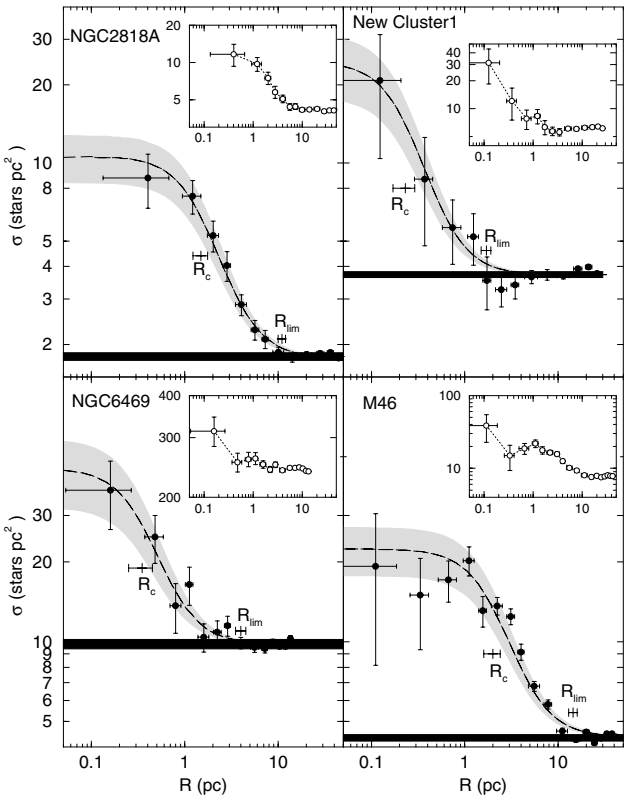

Figure 5. Stellar RDPs (filled circles) of the present star clusters built with colour–magnitude-filtered photometry. Solid line: best-fitting King-like profile. Horizontal shaded region: offset field stellar background level. Grey regions: 1σ King fit uncertainty. The core and limiting radii are indicated. Insets: RDPs built with the observed photometry. Absolute scale is used.

the average position and standard deviation of the stars inside the ring.

The resulting RDPs of the present star clusters are given in Fig. 5. For absolute comparison between clusters the radius scale was converted to parsecs and the number density of stars to stars pc^{-2} for the distances derived in Section 3.2. Besides the RDPs resulting from the colour–magnitude filters, we also show, for illustrative purposes, those produced with the observed (raw) photometry. In all cases, minimization of the number of non-cluster stars by the colour–magnitude filter resulted in RDPs with a significantly higher contrast with respect to the background. Fits of the King-like profile were performed with a non-linear least-squares fit routine that uses errors as weights. To minimize degrees of freedom, σ_0 and R_c were derived from the RDP fit, while σ_{bg} is measured in the respective comparison field. These values are given in Table 4, and the best-fitting solutions are superimposed on the colour–magnitude-filtered RDPs (Fig. 5). Because of the 2MASS photometric limit, which in most cases corresponds to a cut-off for stars brighter than $J \approx 15$, σ_0 should be taken as a lower limit to the actual central number density. The adopted King-like function describes well the RDPs throughout the full radii range, within uncertainties.

We also estimate the cluster limiting radius and uncertainty by visually comparing the RDP level (taking into account fluctuations) with the background. In this sense, R_l corresponds to the distance from the cluster centre where RDP and background become statistically indistinguishable from each other (e.g. Bonatto & Bica 2005, and references therein). For practical purposes, most of the cluster stars can be considered to be contained within R_l. Note that R_l should not be mistaken for the tidal radius. For instance, in populous and relatively high Galactic latitude OCs such as M 26, M 67, NGC 188 and 2477, limiting radii are a factor of ∼0.5–0.7 of the respective tidal radii (Bonatto & Bica 2005). The limiting radii of the present objects are given in column 7 of Table 4. Tidal radii are derived from fits of King profile to RDPs, which depend on wide surrounding fields and adequate Poisson errors. If limiting and tidal radii of the present clusters are similarly related as for the bright ones, we note that, in all cases, the lower limit of the radial range adopted as comparison field (Section 3.1) is located beyond the respective probable tidal radius. This, in turn, minimizes the probability of cluster members at large radii, e.g. in the halo, to be considered as field stars by the decontamination algorithm.

Table 4 (column 5) also provides the density contrast parameter $\delta_c = 1 + \sigma_0/\sigma_{bg}$. Since δ_c is measured in colour–magnitude-filtered RDPs, it does not necessarily correspond to the visual contrast produced by observed stellar distributions in images (Figs 1 and 2). NGC 6469, for instance, presents a very low contrast in the DSS *B* image (Fig. 2) but, because most of the non-cluster stars have been excluded by the colour–magnitude filter, the corresponding RDP presents a relatively high density contrast, $\delta_c \approx 4.6$. The same applies to the non-populous OC New Cluster 1.

Probably because of different methods and data sets, the present values of R_c and R_l are different from those in common with Kharchenko et al. (2005). The difference, especially in R_c, may be attributed to their brighter limits (Kharchenko et al. 2004) producing shallower profiles for the bulge-contaminated cluster NGC 6469.

4.1 Mass density profiles

To complete the structural description of the objects we take the mass–luminosity (ML) relation derived from isochrone fits

Table 4. Structural parameters of evolved + MS stars (colour–magnitude-filtered photometry).

			RDP				MDP	
Cluster	1 arcmin	σ_{bg}	σ_0	δ_c	R_c	R_l	σ_0	R_c
	(pc)	(stars pc^{-2})	(stars pc^{-2})		(pc)	(pc)	($M_\odot$ pc^{-2})	(pc)
(1)	(2)	(3)	(4)	(5)	(6)	(7)	(8)	(9)
NGC 2818A	0.805	1.8 ± 0.1	8.8 ± 2.2	5.9 ± 1.2	1.5 ± 0.3	11 ± 1	13.4 ± 1.8	1.5 ± 0.2
M 46	0.442	4.4 ± 0.1	18.8 ± 4.6	5.1 ± 1.0	2.0 ± 0.4	12.4 ± 0.8	30.8 ± 6.9	2.0 ± 0.3
NGC 6469	0.318	9.8 ± 0.2	35.3 ± 13.0	4.6 ± 0.5	0.35 ± 0.10	4.0 ± 0.5	49 ± 8	0.45 ± 0.10
New Cluster 1	0.493	3.7 ± 0.1	20.8 ± 6.6	6.6 ± 1.8	0.23 ± 0.06	1.7 ± 0.2	27.9 ± 1.6	0.25 ± 0.02

Notes: Column 2: arcmin to parsec scale. King profile is expressed as $\sigma(R) = \sigma_{bg} + \sigma_0/[1 + (R/R_{core})^2]$. To minimize degrees of freedom in RDP fits, σ_{bg} was kept fixed (measured in the respective comparison fields) while σ_0 and R_c were allowed to vary. MDPs are background subtracted profiles. Column 5: cluster/background density contrast ($\delta_c = 1 + \sigma_0/\sigma_{bg}$), measured in colour–magnitude-filtered RDPs.

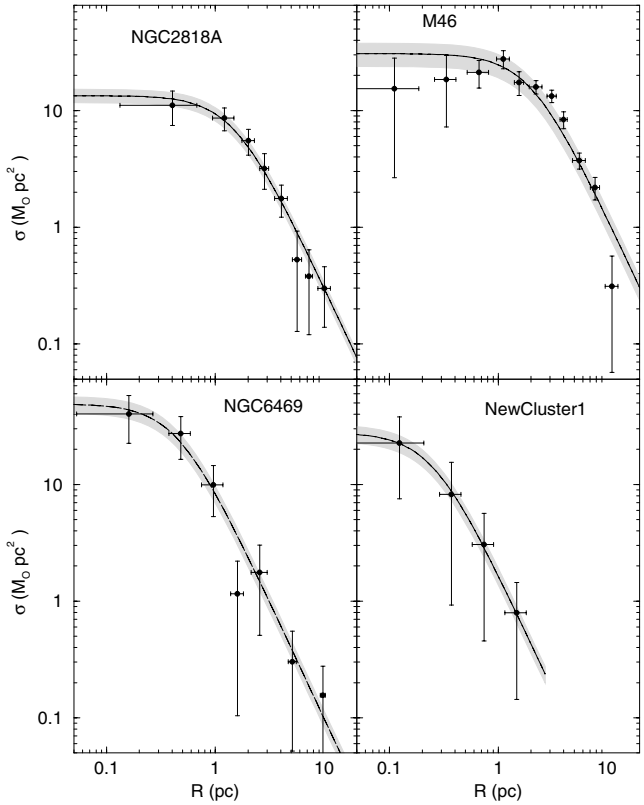

Figure 6. Same as Fig. 5 for the MDPs. The background contribution has been subtracted.

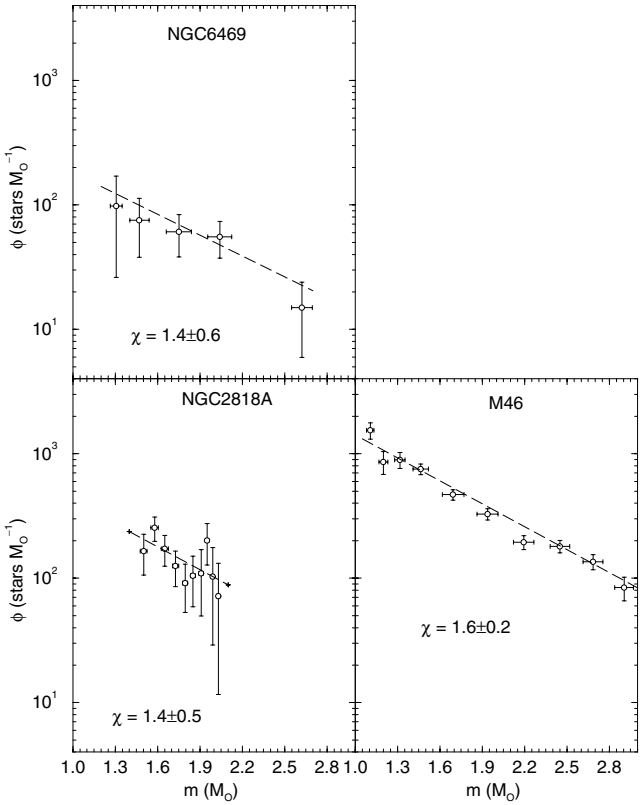

Figure 7. Overall MFs fitted with $\phi(m) \propto m^{-(1+\chi)}$. Within the uncertainties, the MF slopes are similar to Salpeter IMF.

(Section 3.2) to build statistical MDPs. We follow the same systematics as that used to build RDPs. Instead of computing the number density of stars in rings, we now assign each star a mass according to the respective ML relation. MDPs are produced by subtracting from the mass density in each ring that measured in the comparison field. They are shown in Fig. 6, together with the respective King-like fits. Likewise RDPs, MDPs are well described by King-like profiles. Core radii derived from MDPs (column 9 of Table 4) agree, at 1σ, with RDP ones (column 6).

5 MASS FUNCTIONS AND CLUSTER MASS

The methods presented in Bonatto & Bica (2005) (and references therein) are used to build the MFs, $[\phi(m) = \mathrm{d}N/\mathrm{d}m]$. We build them with colour–magnitude-filtered photometry, the three 2MASS bands separately, and the ML relations obtained from the respective Padova isochrones and distances from the Sun (Section 3.2). Further details on MF construction are given in Bica et al. (2006a). The effective magnitude range over which MFs are computed is that where clusters present an excess of stars with respect to the comparison field. In all cases it begins right below the TO and ends at a faint magnitude limit brighter than that stipulated by the 2MASS completeness limit (Section 3). The effective MS stellar mass ranges are $1.1 \leqslant m(\mathrm{M}_\odot) \leqslant 2.1$ (NGC 2818A), $1.1 \leqslant m(\mathrm{M}_\odot) \leqslant 3.5$ (M 46), $1.3 \leqslant m(\mathrm{M}_\odot) \leqslant 3.5$ (NGC 6469) and $1.1 \leqslant m(\mathrm{M}_\odot) \leqslant 2.1$ (New Cluster 1). However, we note that because of the non-populous nature of New Cluster 1, the MF error bars resulted exceedingly large.

The resulting MFs are shown in Fig. 7, where fits with the function $\phi(m) \propto m^{-(1+\chi)}$ are included; MF slopes are given in column 4 of Table 5. The populous nature of M 46 allowed computation of the core and halo MF parameters; for NGC 2818A and NGC 6469, only the overall MF was considered. Within uncertainties, the MFs of the present clusters have slopes similar to that of Salpeter (1955) initial mass function (IMF) ($\chi = 1.35$). The core MF of M 46 appears flatter than that of the halo.

Table 5 gives parameters of the target clusters measured in the CMDs and derived from MFs. The number of evolved stars (column 2) was obtained by integration of the (background-subtracted) colour–magnitude-filtered luminosity function for stars brighter than the TO. This number multiplied by the stellar mass at the TO yields an estimate of the mass stored in evolved stars (column 3). The number and mass of the observed MS stars (columns 5 and 6, respectively) were derived by integrating the MFs over the effective MS mass range.

To estimate the total stellar mass we extrapolate the observed MFs down to the H-burning mass limit ($0.08\,\mathrm{M}_\odot$). For masses below the present detection threshold (Table 5) we base the extrapolation on Kroupa (2001) universal IMF, in which $\chi = 0.3 \pm 0.5$ for the range $0.08 \leqslant m(\mathrm{M}_\odot) \leqslant 0.5$ and $\chi = 1.3 \pm 0.3$ for $0.5 \leqslant m(\mathrm{M}_\odot) \leqslant 1.0$. When the present MF slopes are flatter than or similar (within uncertainties) to the Kroupa MF slopes, we adopt the measured values of χ. The total (extrapolated MS + evolved) values of number, mass, surface and volume densities are given in columns 7–10 of Table 5.

The mass stored in the observed MS and evolved stars of M 46 amounts to $M_{\mathrm{obs}} \sim 1\,500\,\mathrm{M}_\odot$, compatible with the populous CMD (Fig. 3). The present observed mass estimate for NGC 2818A, $M_{\mathrm{obs}} \approx 240\,\mathrm{M}_\odot$ agrees with the estimate of Tadross et al. (2002). NGC 6469, and especially New Cluster 1, are low-mass OCs, respectively, with $M_{\mathrm{obs}} \approx 120$ and $30\,\mathrm{M}_\odot$. The extrapolated masses

Table 5. Parameters related to cluster mass and stellar population.

Region	Evolved		Observed MS			Evolved + extrapolated MS			
	N^* (stars)	m ($M_\odot$)	χ	N^* (stars)	m_{obs} ($M_\odot$)	N^* (10^2 stars)	m ($10^2\,M_\odot$)	σ ($M_\odot\,pc^{-2}$)	ρ ($M_\odot\,pc^{-3}$)
(1)	(2)	(3)	(4)	(5)	(6)	(7)	(8)	(9)	(10)
NGC 2818A – MS: $1.1 \leqslant m(M_\odot) \leqslant 2.1$ – Age $= 1.0 \pm 0.1$ Gyr}									
Core	6 ± 1	14 ± 3	–	24 ± 5	40 ± 5	–	–	–	–
Halo	18 ± 8	38 ± 18	–	90 ± 20	149 ± 20	–	–	–	–
Overall	25 ± 9	52 ± 18	1.44 ± 0.55	115 ± 20	189 ± 21	41 ± 36	15 ± 8	3.9 ± 2.0	0.26 ± 0.14
M 46 – MS: $1.1 \leqslant m(M_\odot) \leqslant 3.5$ – Age $= 250 \pm 50$ Myr									
Core	9 ± 2	29 ± 6	1.31 ± 0.50	133 ± 15	214 ± 14	17 ± 13	7 ± 3	55 ± 21	21 ± 8
Halo	22 ± 6	68 ± 19	1.60 ± 0.22	727 ± 70	1147 ± 56	112 ± 83	43 ± 16	9.0 ± 3.3	0.54 ± 0.20
Overall	32 ± 6	98 ± 20	1.63 ± 0.15	860 ± 71	1362 ± 58	135 ± 99	51 ± 18	10.6 ± 3.8	0.64 ± 0.23
NGC 6469 – MS: $1.3 \leqslant m(M_\odot) \leqslant 3.5$ – Age $= 250 \pm 50$ Myr									
Core	–	–	–	9 ± 4	15 ± 3	–	–	–	–
Halo	–	–	–	65 ± 31	107 ± 28	–	–	–	–
Overall	1 ± 1	2 ± 2	1.38 ± 0.63	74 ± 31	122 ± 29	16 ± 13	6.3 ± 2.8	13 ± 6	2.4 ± 1.0
New Cluster 1 – MS: $1.1 \leqslant m(M_\odot) \leqslant 2.1$ – Age $= 1.0 \pm 0.1$ Gyr									
Core	–	–	–	–	–	–	–	–	–
Halo	–	–	–	–	–	–	–	–	–
Overall	7 ± 2	14 ± 4	–	13 ± 8	18 ± 7	–	–	–	–

Notes: Column 6: stellar mass stored in the observed MS; column 8: mass of the evolved stars added to the MS mass extrapolated to 0.08 $M_\odot$.

are a factor of ∼5 times larger than the observed ones. As a caveat we note that the total mass estimates should be taken as upper limits, since because of dynamical evolution, significant fractions of the low-mass content may have been lost to the field.

6 COMPARISON WITH NEARBY OCS

At this point it is interesting to compare the structural parameters derived for the present OCs with those of a reference sample of nearby OCs with ages in the range 70–7000 Myr and masses within 400–5300 $M_\odot$ (Bonatto & Bica 2005). To the original reference sample were added the young OCs NGC 6611 (Bonatto et al. 2006a) and NGC 4755 (Bonatto et al. 2006c). Clusters are differentiated according to total mass (smaller or larger than 1000 $M_\odot$). Details on parameter correlation in the reference sample are given in Bonatto & Bica (2005).

In panels (a) and (b) of Fig. 8 we compare limiting and core radii of the present OCs with those of the reference sample in terms of cluster age. With respect to both kinds of radii, the bulge-projected NGC 6469 and the poorly populated New Cluster 1 appear to be significantly smaller than the nearby OCs of similar ages, especially in limiting radius. Core and limiting radii in the reference sample are related by $R_l = (8.9 \pm 0.3) \times R_{core}^{(1.0\pm0.1)}$ (panel c), which suggests a similar scaling for both kinds of radii, at least for the radii ranges $0.5 \lesssim R_c(pc) \lesssim 1.5$ and $5 \lesssim R_l(pc) \lesssim 15$. Within uncertainties, NGC 2818A, M 46, NGC 6469 and New Cluster 1 also follow that relation. Finally, except for New Cluster 1, the remaining OCs appear to follow the trend of increasing limiting radii with Galactocentric distance (panel d). A similar dependence with R_{GC} holds as well for R_c, because of the relation implied by panel (c).

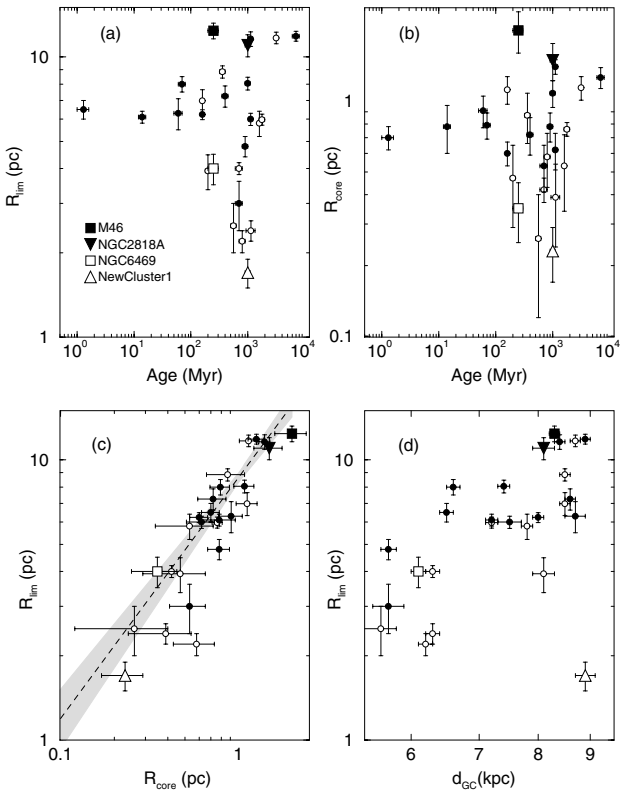

Figure 8. Relations involving structural parameters of OCs. Circles: nearby OCs, including two young ones. Filled symbols: OCs more massive than 1000 $M_\odot$.

7 DISCUSSION

Besides the spatial coincidence, for a physical association between a PN and a star cluster to be considered as highly probable, at least the radial velocities, reddening values and distances should be compatible. In the present work we derive reliable values of reddening, distance from the Sun, core and limiting radii for the OCs. The angular separation of the PNe NGC 2818, 2438 and PK 6+2.5 with respect to the OC centres (Table 2), corresponds to the halo; PK 167−0.1,

on the other hand, appears to lie near the border of New Cluster 1. In all cases, the mass at the TO of the OC is consistent with the presence of a PN.

Based on the above criteria, the best candidate to a physical pair is the PN NGC 2438 with the OC M 46. They have comparable radial velocities (Section 2.1), and the reddening and distance from the Sun for the PN are $E(B-V) = 0.17 \pm 0.08$ and $d_\odot \sim 1.8$ kpc (Section 2.1), while for the OC we derive $E(B-V) = 0.10 \pm 0.03$ and $d_\odot = 1.5 \pm 0.1$ kpc. Besides, the presence of a PN in M 46 is compatible with the TO mass, $m_{TO} \approx 3.5\,M_\odot$.

Within uncertainties, the present reddening $E(B-V) = 0.10 \pm 0.03$ for the OC NGC 2818A is compatible with the $E(B-V) = 0.18$ and $E(B-V) = 0.28 \pm 0.15$ (Section 2.1) for the PN NGC 2818. Distances from the Sun are in better agreement, $d_\odot = 2.8 \pm 0.1$ kpc for NGC 2818A and $d_\odot = 2.3$–2.7 kpc for NGC 2818 (Section 2.1). However, the radial velocities do not agree (Section 2.1), which could indicate a projection effect.

PK 6+2.5 does not appear to be physically associated with NGC 6469. If this nearby cluster (Table 1) has a circular orbit about the Galactic Centre, a small value for its radial velocity is expected from its Galactic location. However, the relatively high velocity $V_r = 68.8 \pm 1.8\,km\,s^{-1}$ (Section 2.3) of PK 6+2.5 suggests rather a relation to the bulge.

The distance of 1780 pc of PK 167−0.1 (Section 2.4) is in excellent agreement with that derived for New Cluster 1, $d_\odot = 1.7 \pm 0.1$ kpc (Table 1). This piece of evidence suggests physical association, but the cluster radial velocity should be determined for a more robust comparison.

Majaess et al. (2007) comment that most potential PNe in OCs are projected against the cluster halo. At least in part, this observation can be a direct consequence of the relatively high cluster halo/core cross-section ratio, $A_h/A_c = (R_l - R_c)^2/R_c^2$. Indeed, from Fig. 8 (panel c) it follows that the limiting and core radii are related by $R_l \approx 9\,R_c$, which implies that, for a typical OC, $A_h/A_c \approx 60$. In this sense, random distributions of (spatially unrelated) PNe and OCs would result in a significantly larger number of PNe projected against haloes than central regions. For the 30 spatial coincidences (with separation $\Delta R < 15$ arcmin), Majaess et al. (2007) present an estimate of a nuclear radius (r_n) and measure the angular separation of the PN with respect to the cluster centre. Although their r_n is not derived from radial profiles, it probably represents the core radius to some degree. For the two additional pairs dealt with in the present paper, the ratio of the number of cluster halo/core PNe is $N_h/N_c \approx 26/6 = 4.3$, less than 10 per cent of that expected of random, unrelated distributions. Interestingly, for a King-like cluster characterized by the core and limiting radii R_c and R_l, the number of member stars in the halo is related to that in the core by $N_h/N_c = \ln[1 + (R_l/R_c)^2]/\ln(2) - 1$. Thus, for $R_l \approx 9\,R_c$, we obtain $N_h/N_c \approx 5.4$, close to the corresponding observed ratio for the PNe of Majaess et al. (2007).

We further examine this issue from a different perspective, similar to that employed by Lundström & Stenholm (1984) to study spatial coincidences of WR stars with OCs. We compute the ratio of the PN/OC separation to the cluster apparent radius $\chi = \Delta R/R_{OC}$, based on the angular diameters given by Dias et al. (2002). According to this definition, χ represents the PN separation as a function of the apparent cluster radius. Next we build the surface density distribution of the measured χ values, i.e. the number of spatial coincidences characterized by χ per cluster area, which is shown in Fig. 9. To investigate the significance of this distribution we first test whether it could result from a random spatial distribution of PNe. The 30 PN/OC angular separations in Majaess et al. (2007),

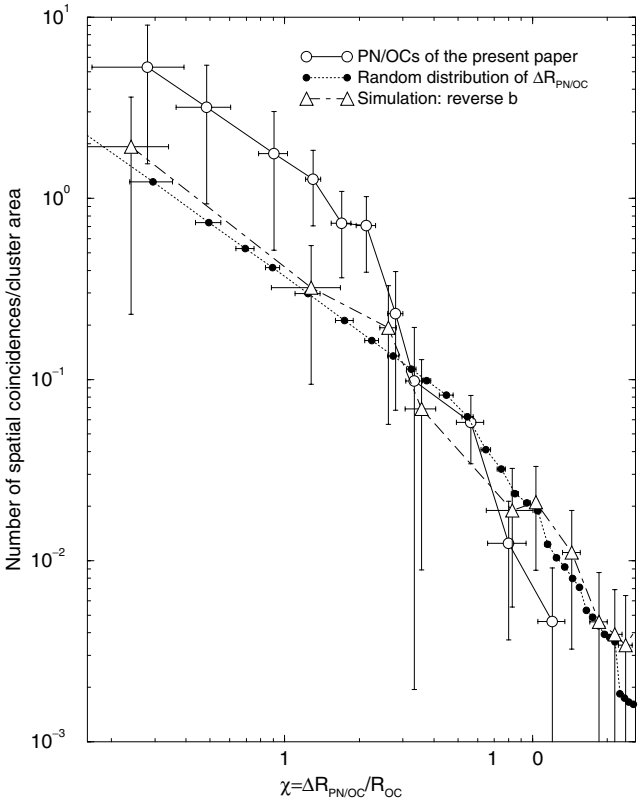

Figure 9. Surface density distribution (number of spatial coincidences characterized by χ per cluster area). Empty circles: the 32 spatial coincidences in this paper. Filled circles: distribution simulated with 10^6 values of ΔR, randomly taken from the range 0–55 arcmin, divided by the actual apparent cluster radii. Empty triangles: distribution of the 20 spatial coincidences that result after reversion of the sign of PN's b coordinate. The latter two distributions were normalized to 32 objects. The apparent cluster radii (Dias et al. 2002) are around two to three times smaller than the limiting radii.

and the two additional ones (Table 2) not in common with them, are restricted to $\Delta R \lesssim 55$ arcmin. For each of the 32 OCs corresponding to the above spatial coincidences, we randomly take values of ΔR uniformly distributed in the range $0 \lesssim \Delta R \lesssim 55$ arcmin and compute χ for the actual apparent OC radius. The respective surface density distribution was built for 10^6 runs, which was subsequently normalized to 32 objects. The measured curve presents a conspicuous excess over the simulated one for $\chi \lesssim 3$, which might indicate a physical relation. Both curves agree for $\chi \gtrsim 3$, within the uncertainties. The second test follows Lundström & Stenholm (1984): the sign of the Galactic latitude (b) of each PN is reversed, but keeping the original ℓ. Based on the new PN coordinates, we then searched for an OC that is closer than $\Delta R \lesssim 55$ arcmin, a condition that was matched for 20 cases. Within the uncertainties, the corresponding surface density distribution, normalized to 32 objects (Fig. 9), coincides with the simulated (random spatial distribution of ΔR values) one along the full range of χ.

The arguments above are based on the apparent cluster radii of Dias et al. (2002). Because they are basically visually determined, such radii, however, are significantly underestimated with respect to the limiting radii and, especially, the tidal radii. For instance, the OCs in Bica et al. (2006a), Bonatto & Bica (2006, 2007) and Bonatto et al. (2006c), which are similar to those in Majaess et al. (2007) and were studied with the same methods as in the present paper, have a limiting radius around two to three times larger than

the apparent radius given in Dias et al. (2002). Thus, if a similar relation holds for the apparent and limiting radii in the present OC sample, the excess in the observed surface density (Fig. 9) would correspond to PN separations $\Delta R \lesssim R_l \ll R_t$, which again suggests a physical relation.

Despite the many uncertainties associated with the above arguments, the small number of targets and the uncertain PN distances in particular, it might, nevertheless, be speculated whether the relatively large fraction of core PNe results from a physical relation. A cautionary remark is that the remaining spatial coincidences in Majaess et al. (2007) should be analysed in detail for a better definition of the core and limiting radii, as well as the fundamental parameters.

8 SUMMARY AND CONCLUSIONS

In the present study an OC was discovered (New Cluster 1), which is located at $\alpha(J2000) = 05^h06^m20^s$ and $\delta(J2000) = +39^\circ09'50''$. Projected on its field, with an angular separation of 4.9 arcmin with respect to the custer centre, is the PN PK 167−0.1. Field-star-decontaminated 2MASS photometry was employed in the analysis of four pairs of PN/OC candidates to physical association. We derived accurate ages, distances from the Sun, reddening values and the mass at the TO for the clusters. Cluster core and limiting radii were determined by means of RDPs fitted with a King-like function.

The values of reddening and distance from the Sun derived in this work suggest that the pairs PN/OC NGC 2818/2818A and NGC 2438/M46 are compatible with physical associations. However, the available radial velocity data for NGC 2818/2818A favour a projection effect. The pair PK 6+2.5/NGC 6469 appears to be physically unrelated, since the radial velocity of PK 6+2.5 suggests a bulge membership. The PN PK 167−0.1 is projected close to the OC New Cluster 1, and the similar distances are consistent with physical association. In the cases of physical association, the TO masses are compatible with the occurrence of PNe. It would be important to determine radial velocities for members of the new cluster, to compare them with that of PK 167−0.1, in order to further test the physical association possibility. Besides, to establish the non-association of PK 6+2.5 with NGC 6469, radial velocities of member stars are necessary.

From the PN/OC angular positions provided by Majaess et al. (2007), we estimate that the fraction of PNe projected against the central region of clusters, with respect to those in the halo, is significantly higher than that expected from spatially unrelated distributions of PNe and OCs. Besides, this fraction agrees with that expected of clusters characterized by a King-like radial stellar distribution. In addition, we analysed the distribution of the number of spatial coincidences per cluster area built with the 32 cases dealt with in this paper. This curve was compared to that expected from a spatially unrelated distribution of PN/OC separations and that resulting from inversion of the sign of the b PN coordinates. The observed distribution presents a conspicuous excess, for PN/OC separations smaller than the cluster limiting radii, over both simulations, which might indicate a physical relation. However, we note that these results do not take into account the rather uncertain PN distances and radial velocities. Besides, they are based on a relatively small number of spatial coincidences. In this context, it is essential to analyse in more detail (i.e. with accurate fundamental and structural parameters) the whole PN/OC sample of Majaess et al. (2007) in order to investigate whether the above excess of relatively close spatial coincidences can be interpreted as physical association.

ACKNOWLEDGMENTS

We thank the referee for suggestions. This publication makes use of data products from the 2MASS, which is a joint project of the University of Massachusetts and the Infrared Processing and Analysis Center/California Institute of Technology, funded by the National Aeronautics and Space Administration and the National Science Foundation. This research has made use of the WEBDA data base, operated at the Institute for Astronomy of the University of Vienna. We acknowledge support from the Brazilian Institution CNPq.

REFERENCES

Bessel M. S., Brett J. M., 1988, PASP, 100, 1134
Bica E., Bonatto C., 2005, A&A, 443, 465
Bica E., Bonatto C., Dutra C. M., 2003, A&A, 405, 991
Bica E., Bonatto C., Dutra C. M., 2004, A&A, 422, 555
Bica E., Bonatto C., Blumberg R., 2006a, A&A, 460, 83
Bica E., Bonatto C., Barbuy B., Ortolani S., 2006b, A&A, 450, 105
Bica E., Bonatto C., Camargo D., 2007, MNRAS, preprint (arXiv:0712.0762)
Bonatto C., Bica E., 2005, A&A, 437, 483
Bonatto C., Bica E., 2006, A&A, 455, 931
Bonatto C., Bica E., 2007, MNRAS, 377, 1301
Bonatto C., Bica E., Girardi L., 2004, A&A, 415, 571
Bonatto C., Bica E., Santos J. F. C. Jr, 2005, A&A, 433, 917
Bonatto C., Santos J. F. C. Jr, Bica E., 2006a, A&A, 445, 567
Bonatto C., Kerber L. O., Bica E., Santiago B. X., 2006b, A&A, 446, 121
Bonatto C., Bica E., Ortolani S., Barbuy B., 2006c, A&A, 453, 121
Dias W. S., Alessi B. S., Moitinho A., Lépine J. R. D., 2002, A&A, 389, 871
Durand S., Acker A., Zijlstra A., 1998, A&AS, 132, 13
Dutra C. M., Santiago B. X., Bica E., 2002, A&A, 383, 219
Eisenhauer F., Schödel R., Genzel R., Ott T., Tecza M., Abuter R., Eckart A., Alexander T., 2003, ApJ, 597, L121
Eisenhauer F. et al., 2005, ApJ, 628, 246
Elson R. A. W., Fall S. M., Freeman K. C., 1987, ApJ, 323, 54
Girardi L., Bertelli G., Bressan A., Chiosi C., Groenewegen M. A. T., Marigo P., Salasnich B., Weiss A., 2002, A&A, 391, 195
Hurley J., Tout A. A., 1998, MNRAS, 300, 977
Kerber L. O., Santiago B. X., Castro R., Valls-Gabaud D., 2002, A&A, 390, 121
Kharchenko N. V., Piskunov A. E., Röser S., Schilbach E., Scholz R.-D., 2004, Astron. Nachr., 325, 740
Kharchenko N. V., Piskunov A. E., Röser S., Schilbach E., Scholz R.-D., 2005, A&A, 438, 1163
King I., 1962, AJ, 67, 471
King I., 1966, AJ, 71, 64
Köppen J., Acker A., 2000, in Lançon A., Boily C., eds, ASP Conf. Ser. Vol. 211, Massive Stellar Clusters. Astron. Soc. Pac., San Francisco, p. 151
Kroupa P., 2001, MNRAS, 322, 231
Lada C. J., Lada E. A., 2003, ARA&A, 41, 57
Lata S., Pandey A. K., Sagar R., Mohan V., 2002, A&A, 388, 158
Lundström I., Stenholm B., 1984, A&AS, 58, 163
Majaess D. J., Turner D. G., Lane D. J., 2007, PASP, 119, 1349
Meatheringham S. J., Wood, P. R., Faulkner D. J., 1988, ApJ, 334, 862
Mermilliod J. C., Clariá J. J., Andersen J., Piatti A. E., Mayor M., 2001, A&A, 375, 30
Mermilliod J. C., Paunzen E., 2003, A&A, 410, 511
Meynet G., Mermilliod J.-C., Maeder A., 1993, A&AS, 98, 477
Moe M., De Marco O., 2006, ApJ, 650, 916
Nilakshi S. R., Pandey A. K., Mohan V., 2002, A&A, 383, 153
Nishiyama S. et al., 2006, ApJ, 647, 1093
Pauls R., Kohoutek L., 1996, Astron. Nachr., 317, 413
Pedreros M., 1989, AJ, 98, 2146
Phillips J. P., 2004, MNRAS, 353, 589
Salpeter E., 1955, ApJ, 121, 161
Santos J. F. C. Jr, Bonatto C., Bica E., 2005, A&A, 442, 201

Schönberner D., Blöcker T., 1996, Ap&SS, 245, 201
Sharma S., Pandey A. K., Ogura K., Mito H., Tarusawa K., Sagar R., 2006, AJ, 132, 1669
Skrutskie M. et al., 1997, in Garzon F., Epchtein N., Omont A., Burton B., Persi P., eds, Astrophys. & Space Sci. Libr. Vol. 210, The Impact of Large Scale Near-IR Sky Surveys. Kluwer, Dordrecht, p. 25
Soker N., 2006, ApJ, 645, L57
Tadross A. L., Werner P., Osman A., Marie M., 2002, New Astron., 7, 553
Tylenda R., Acker A., Stenholm B., Köppen J., 1992, A&AS, 95, 337
Weidemann V., 2000, A&A, 363, 647
Wilson C. P., 1975, AJ, 80, 175
Zhang C. Y., 1995, ApJS, 98, 659
Zijlstra A. A., 2007, Balt. Astron., 16, 79
ŽiNovský J., 1975, Bull. Astron. Inst. Czech., 26, 248

This paper has been typeset from a TEX/LATEX file prepared by the author.